Concurrence of monoenergetic electron beams and bright X-rays from an evolving laser-plasma bubble

Wenchao Yan[a], Liming Chen[a,1], Dazhang Li[b], Lu Zhang[a], Nasr A. M. Hafz[c], James Dunn[d], Yong Ma[a], Kai Huang[a], Luning Su[a], Min Chen[c], Zhengming Sheng[c,e], and Jie Zhang[c,1]

[a]Beijing National Laboratory for Condensed Matter Physics, Institute of Physics, Chinese Academy of Sciences, Beijing 100190, China; [b]Institute of High Energy Physics, Chinese Academy of Sciences, Beijing 100049, China; [c]Key Laboratory for Laser Plasmas (Ministry of Education), Department of Physics and Astronomy, Shanghai Jiao Tong University, Shanghai 200240, China; [d]Lawrence Livermore National Laboratory, CA 94550; and [e]Scottish Universities Physics Alliance, Department of Physics, University of Strathclyde, Glasgow G4 0NG, United Kingdom

Contributed by Jie Zhang, March 6, 2014 (sent for review October 20, 2013)

Desktop laser plasma acceleration has proven to be able to generate gigaelectronvolt-level quasi-monoenergetic electron beams. Moreover, such electron beams can oscillate transversely (wiggling motion) in the laser-produced plasma bubble/channel and emit collimated ultrashort X-ray flashes known as betatron radiation with photon energy ranging from kiloelectronvolts to megaelectronvolts. This implies that usually one cannot obtain bright betatron X-rays and high-quality electron beams with low emittance and small energy spread simultaneously in the same accelerating wave bucket. Here, we report the first (to our knowledge) experimental observation of two distinct electron bunches in a single laser shot, one featured with quasi-monoenergetic spectrum and another with continuous spectrum along with large emittance. The latter is able to generate high-flux betatron X-rays. Such is observed only when the laser self-guiding is extended over 4 mm at a fixed plasma density (4×10^{18} cm^{-3}). Numerical simulation reveals that two bunches of electrons are injected at different stages due to the bubble evolution. The first bunch is injected at the beginning to form a stable quasi-monoenergetic electron beam, whereas the second one is injected later due to the oscillation of the bubble size as a result of the change of the laser spot size during the propagation. Due to the inherent temporal synchronization, this unique electron–photon source can be ideal for pump–probe applications with femtosecond time resolution.

Synchrotron light sources are powerful in generating bright X-rays for a wide range of applications in basic science, medicine, and industry (1). However, these machines are usually large in size and expensive for construction and maintenance and are thus unaffordable to many would-be users. With the advent of tabletop ultrashort and ultraintense lasers, laser plasma acceleration (LPA) proposed by Tajima and Dawson (2) has demonstrated its great potential as a compact accelerator and X-ray source. Significant progress in LPA was made in the last decade (3–11): Well-collimated (approximately millirad) quasi-monoenergetic electron beams were first observed in 2004, and the electron energy above gigaelectronvolts over centimeter-scale acceleration lengths were demonstrated in several laboratories in the last few years.

While accelerating longitudinally in the laser wakefield, the electron beams also oscillate transversally (wiggling motion) due to the transverse structure of the wakefield, which emits well-collimated betatron X-rays (12–14). Among several mechanisms to generate X-ray radiation from laser–plasma interactions (15–20), betatron radiation is straightforward and able to deliver larger X-ray photon fluxes per shot [$\sim 10^8$ phs/shot (21)] and higher photon energies [up to gamma rays (22)]. The betatron oscillation frequency is given by $\omega_\beta = \omega_p(2\gamma)^{-1/2}$, where ω_p is the plasma frequency and γ is the Lorentz factor of the accelerated electron beam. For large-amplitude betatron oscillations (i.e., a few micrometers in size), the resulting broadband spectrum extends up to the critical frequency of $\omega_c \sim 2\gamma^2\omega_\beta$, after which it drops exponentially. The radiation is emitted in the forward direction within a cone angle $\theta \sim K/\gamma$, where K is the strength parameter of the plasma wiggler given by $K = 2\pi(\gamma r_0)/\lambda_b = 1.33 \times 10^{-10}\gamma^{1/2}n_e^{1/2}[\mathrm{cm}^{-3}]r_0[\mu\mathrm{m}]$, and λ_b is the betatron wavelength. The average photon number with mean energy $\hbar\omega_c$ emitted by an electron is given by $N_x = 5.6 \times 10^{-3}\, N_\beta K$, where N_β is the number of oscillation periods. Many experiments (11, 21–25) have been carried out to enhance the radiation flux, for example, to increase the electron charge, the electron energy, the oscillation amplitude r_0, and oscillation period N_β through extending the acceleration length. However, these experiments have shown that the improvement of the betatron X-ray flux is generally accompanied by a loss of electron beam quality. For example, as mentioned above, because $N_x \propto r_0$, the increasing of r_0 is considered an efficient way to enhance the X-ray flux, but this results in a larger electron emittance and energy spread.

Results

In this paper, we demonstrate the simultaneous generation of quasi-monoenergetic electron beams and collimated high flux X-ray sources from multiple injections in self-injected laser wakefield acceleration on a 100-TW laser system using 1-cm-long helium gas jet. Two sequentially injected bunches of electrons are observed in experiment, where the first bunch forms a quasi-monoenergetic spectrum around 0.46 GeV with <9% energy spread and the second bunch contains more electrons but forms a broad spectrum with highest energy up to 1.4 GeV. Such energy is beyond the energy gain estimated by the usual dephasing limit (12). A betatron X-ray flash, which had 4.5×10^8 photons per

Significance

Desktop laser plasma acceleration is able to generate monoenergetic electron beams, and such electron beams can oscillate in the plasma bubble, which results in the collimated X-rays with ability of femtosecond temporal resolution. However, high-flux X-ray emission and high-quality electron beams have not been obtained simultaneously because high-yield X-ray emission is usually produced at the cost of electron beam qualities. By stimulating double injections into a plasma bubble, we report our experimental observation in which both a monoenergetic electron beam at the gigaelectronvolt level and ultraintense hard X-rays with peak brightness higher than the third generation of synchrotrons. Due to the inherent temporal synchronization, this unique electron–photon source can be ideal for "single-shot" pump–probe applications at femtosecond and nanometer scales.

Author contributions: L.C., N.A.M.H., and J.Z. designed research; W.Y., L.C., D.L., L.Z., N.A.M.H., J.D., and L.S. performed research; Y.M., K.H., M.C., and Z.S. contributed new reagents/analytic tools; W.Y., L.C., D.L., Y.M., and K.H. analyzed data; and W.Y., L.C., N.A.M.H., and Z.S. wrote the paper.

The authors declare no conflict of interest.

[1]To whom correspondence may be addressed. E-mail: jzhang1@sjtu.edu.cn or lmchen@iphy.ac.cn.

shot and with critical photon energy ~15 keV, was generated simultaneously at a fixed plasma density (4×10^{18} cm^{-3}). This is higher than the density matched to the blowout regime (26). Two-dimensional particle-in-cell (2D-PIC) simulations illustrate that the experimental observation can be attributed to sequential injections of two electron bunches as the plasma channel length increases. The first injection is found at an early time, which finally forms a stable quasi-monoenergetic electron beam. The second bunch, which contains more electrons, is injected at a later time and produces a continuous spectrum. As the interaction length gets longer, the second beam is accelerated to the gigaelectronvolt level, and the large transverse oscillation amplitude, which is triggered by the oscillation of the laser spot size, results in enhancement of the bright betatron X-ray flux.

The experimental setup is shown in Fig. 1. The laser pulses from a 100-TW laser system are focused on a helium gas jet nozzle (see *Materials and Methods* for details) to create a fully ionized plasma and to excite a relativistic wakefield (plasma wave) that self-traps and accelerates electrons. Because the critical laser power for relativistic self-guiding in the plasma is given by $P_{cr}(\mathrm{GW}) = 17.7\omega^2/\omega_p^2$, at the plasma density of 4×10^{18}cm^{-3} that was used, our laser pulses were well above the self-guiding threshold ($P = 100$ TW $= 13\ P_{cr}$) and can be self-guided over a long distance (>1 cm $\cong 10 z_R$) (27). The dephasing length for the accelerated electrons $L_d \sim \lambda_p^3/\lambda_0^2$ is 7 mm at the above density for 800-nm laser wavelength.

Fig. 2*A* shows a well-collimated (~4 mrad) quasi-monoenergetic electron bunch at 180 MeV ($\Delta E/E \sim 10\%$) that contains 5 pC of charge (see *Materials and Methods* for calibration references); the electron bunch is observed for ~2-mm channel length, as shown in Fig. 2*F*. Betatron radiation was not observed in this case. As we increased the incident laser power, the observed channel length was increased to ~4 mm (Fig. 2*G*). In the meanwhile, the energy of the quasi-monoenergetic electron bunch approaches 290 MeV ($\Delta E/E \sim 20\%$) and a low-energy second bunch starts to appear in the spectrum (Fig. 2*B*). In this laser shot, a weak betatron radiation signal of 2.7×10^7 photons ($E_c \sim 15$ keV) also appears. For a longer channel of 6 mm realized by further increasing the laser power (Fig. 2*H*), the maximum energy of the second electron bunch surpasses the first bunch. From the Fig. 2 *C* and *K*, the two electron bunches overlap in the energy spectra but are still distinguishable, with central energy ~0.43 GeV for first electron bunch and the maximum energy up to 0.6 GeV for the second one. Correspondingly, the betatron radiation becomes much brighter; 1.2×10^8 photons are detected in this shot. As the laser-plasma channel length reaches 9 and 10 mm as shown in Fig. 2 *I* and *J*, the electron bunches accelerated beyond 1 GeV contain 60 and 90 pC of charge, respectively, as shown in Fig. 2 *D* and *E*. *Inset 1* of Fig. 2*K* shows the cutoff (maximum) energy are up to 1.2 and 1.4 GeV with uncertainty of 0.1 GeV at 9- and 10-mm channel lengths, respectively. The energy spectra of these two bunches are obviously broad, however, with peaks around 0.5 and 0.35 GeV, respectively. *Inset 2* of Fig. 2*K* is a typical X-ray beam image with different filters. Considering the attenuating filters between the gas jet and the X-ray detector, the critical energy of the observed betatron radiation (at image plate 3) was around 15 keV (*Materials and Methods*). Moreover, the betatron radiation increases its brightness with the channel length, which is measured with flux of 2.7×10^8 and 4.5×10^8 photons and divergence angles of ~5 and 7 mrad, respectively, for the channel lengths of 9 and 10 mm. These yields of hard X-ray photons represent a ~10-fold enhancement compared with earlier reports (21).

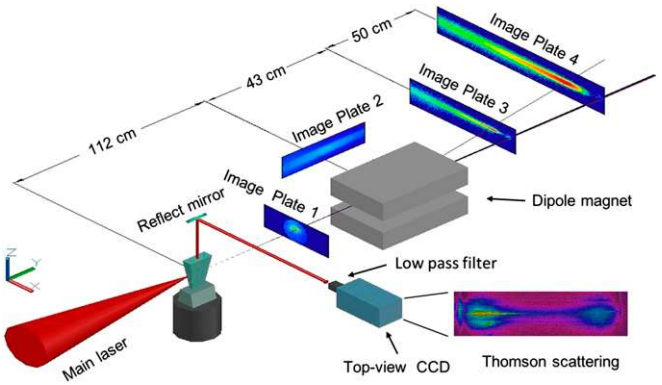

Fig. 1. Schematic of the experimental setup. All image plates were wrapped with 25-μm Al foil. A 1.5-mm-thick Beryllium vacuum window was set 100 cm away from the gas jet to seal the vacuum. The *Lower Right Inset* shows a Thomson scattering image of the plasma channel.

Simulations

To further understand our experimental results, 2D-PIC simulations have been carried out (*Materials and Methods*) using similar laser and target parameters. Different normalized laser amplitudes $a_0 = 2.3$~3.8 have been set in the simulation, corresponding to the peak laser intensity of 1.1×10^{19} to 3.0×10^{19} W·cm^{-2}. When $a_0 = 2.3$, only one electron bunch was injected into a stable bubble to form a quasi-monoenergetic electrons beam. With the increase of a_0, the second electron injection starts to appear. Our simulation illustrates comprehensively the injection and acceleration processes, as shown in Fig. 3 for the electron density (Fig. 3 *A–D*), the longitudinal wakefields and trapped electrons in the longitudinal phase space (Fig. 3 *E–H*), and the longitudinal profiles of the laser field (Fig. 3 *I–L*). At the beginning (Fig. 3 *A* and *E*), a bubble structure surrounded by a high-density sheath of compressed electron fluid is formed immediately behind the laser pulse (28, 29). A bunch of electrons is self-injected and accelerated to ~300 MeV with a narrow energy spread due to the beam-loading effects. At this stage, the bubble structure remains intact and stable, allowing the first bunch to obtain stable acceleration with small-amplitude betatron oscillations. As the laser pulse propagates further into the plasma (Fig. 3 *B* and *F*), the first bunch is now quasi-monoenergetic with a higher energy.

During the laser propagation, the laser pulse front begins to steepen due to the relativistic self-phase modulation and the high-density sheath at the front of the laser pulse (30), as shown in Fig. 3 *I–L*. This steepening in turn leads to a notable increase in the plasma wave amplitude and wavelength, which results in stretching and broadening of the bubble structure as shown in Fig. 3 *C* and *G* at 11.7 ps. At this time, the second wave bucket in the wakefield begins merging with the first bubble to form one large bubble. During this merging process, a second bunch containing more electrons is injected into the large bubble and accelerated to an even higher energy than the first bunch, as shown in Fig. 3 *D* and *H*. At this time, the first quasi-monoenergetic bunch is in the decelerating phase and its maximum energy is reduced. Comparing the simulation in Fig. 3 *D* and *A*, the elongation of plasma wavelength during the bubble evolution makes the dephasing length for the second-injected electron bunch much longer (>1 cm), leading to the higher energy than the normal dephasing limit. In the experiment, we have our laser pulse guided for 1 cm; therefore, a 1.4-GeV maximum electron energy gain is reasonable. This corresponds to the acceleration gradient (1.4 GV/cm) achieved for electrons. Interestingly, the second bunch strongly oscillates up and down at the tail of the large bubble with amplitude as large as about 4 μm, relative to the first electron bunch that experienced negligibly small transverse oscillations (~0.4 μm). The betatron oscillations can

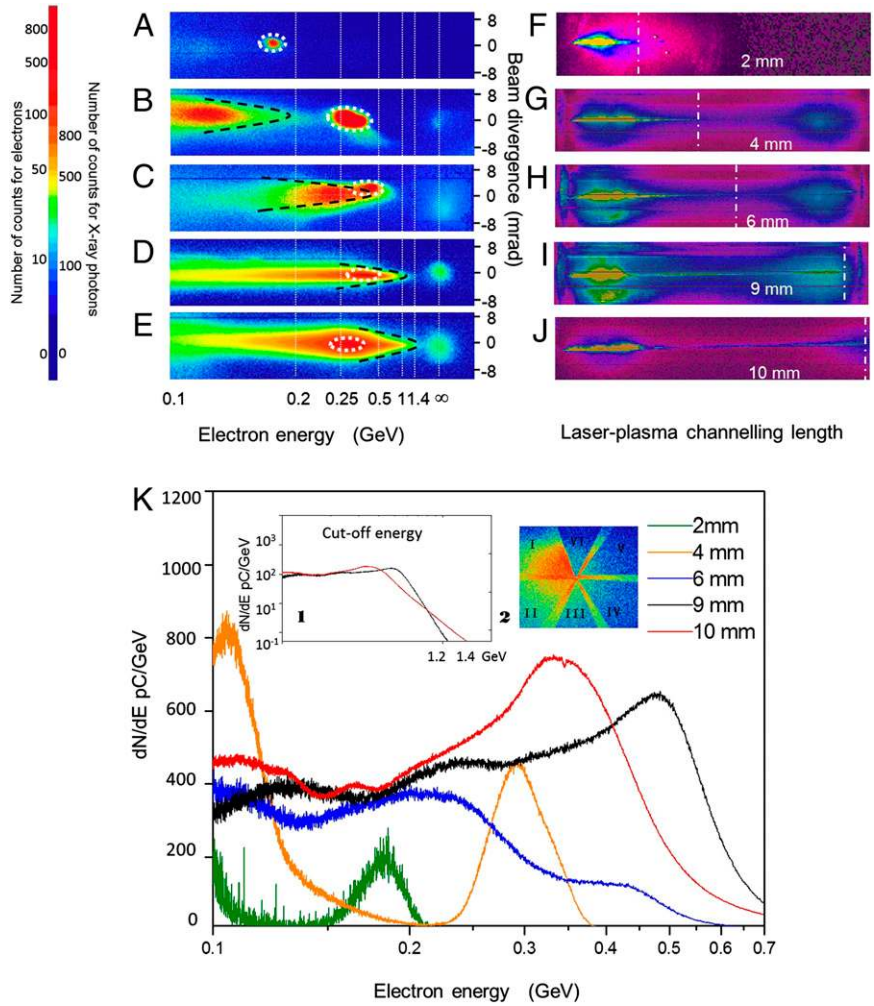

Fig. 2. Accelerated electron beams, betatron X-rays and plasma channel measurement. *A–E* show the spectrum characteristics of the electron beams and the betatron X-ray beam profiles on image plate 3. *F–J* show the corresponding Thomson scattering images obtained from the top view CCD for the nozzle (*F–J*). The normalized peak laser amplitude a_0 in the experiments is 2.6 for *A* and *F*, 2.8 for *B* and *G*, 3.1 for *C* and *H*, 3.3 for *D* and *I*, and 3.6 for *E* and *J*, respectively. *K* is the deconvoluted spectra of electron energy for different channel lengths, where *Inset 1* is the cutoff (maximum) energy spectra of the electrons accelerated beyond 1 GeV. *Inset 2* in *K* is a typical X-ray beam image with different filters, including 78-μm Al (I), 250-μm Al (II), 129-μm Ti (III), 264-μm Ti (IV), 130-μm Cu (V), and 56-μm W (VI).

be found in Fig. 3 *C* and *D* and are traced in Fig. 4 as explained in the following.

Discussion

To understand the injection mechanism for the second electron bunch and the occurrence of the betatron oscillation, we have examined the evolution of the laser spot size from numerical simulations. As shown in Fig. 4, the laser spot size is slowly self-focused to a minimum value at the beginning and then defocused and so on. This kind of oscillation of the laser spot size is typical when the initial matching condition between the laser spot size and the laser amplitude $k_pR \sim k_pw = 2a_0^{1/2}$ is not satisfied (26), where k_p is the plasma wave number, R is the bubble radius, and w is the laser spot size. However, a distinct feature appears later at $t = 8$ ps when the oscillation period of the laser spot size reduces dramatically from 5 to 0.8 ps. Approximately at this time, the injection of the second bunch starts to occur. We call this new injection mechanism "oscillating bubble injection" (OBI) because the laser spot size oscillation causes the transverse oscillation of the bubble. During the OBI, the bubble oscillation can effectively couple to the transverse motion of the second electron bunch by the restoring force in the plasma bubble, starting a betatron resonance. As a result, the betatron transverse oscillation period coincides with the laser spot oscillation period at the beginning of injection. The OBI electrons are injected continuously, resulting in a broad energy spread. Meanwhile, the strong betatron oscillations of the OBI electron bunch lead to the generation of high-flux betatron radiation.

These simulation results agree well with the experimental results for both the electron energy spectra and corresponding betatron characteristics for X-ray emission. As illustrated in Figs. 2 and 3, our numerical simulation and experiment show quite similar features for the generation and evolution of the produced two electron bunches. The first electron bunch is generated and accelerated at the early stage with a quasi-monoenergetic peak (see Fig. 2 *A* and *B* for experiment and Fig. 3 *E* and *F* for simulation), which also experiences deceleration or dephasing at the later stage (Figs. 2 *C–E* and 3 *G* and *H*), whereas the second electron bunch emerges through OBI when the laser pulse starts to evolve violently with its transverse profile oscillating quickly after propagating over 4 mm (see Fig. 2*B* for experiment and Fig. 3*F* for simulation). Because of this oscillation, the transverse momentum of the second bunch is much larger than the first bunch, resulting in a larger divergence angle as observed in the

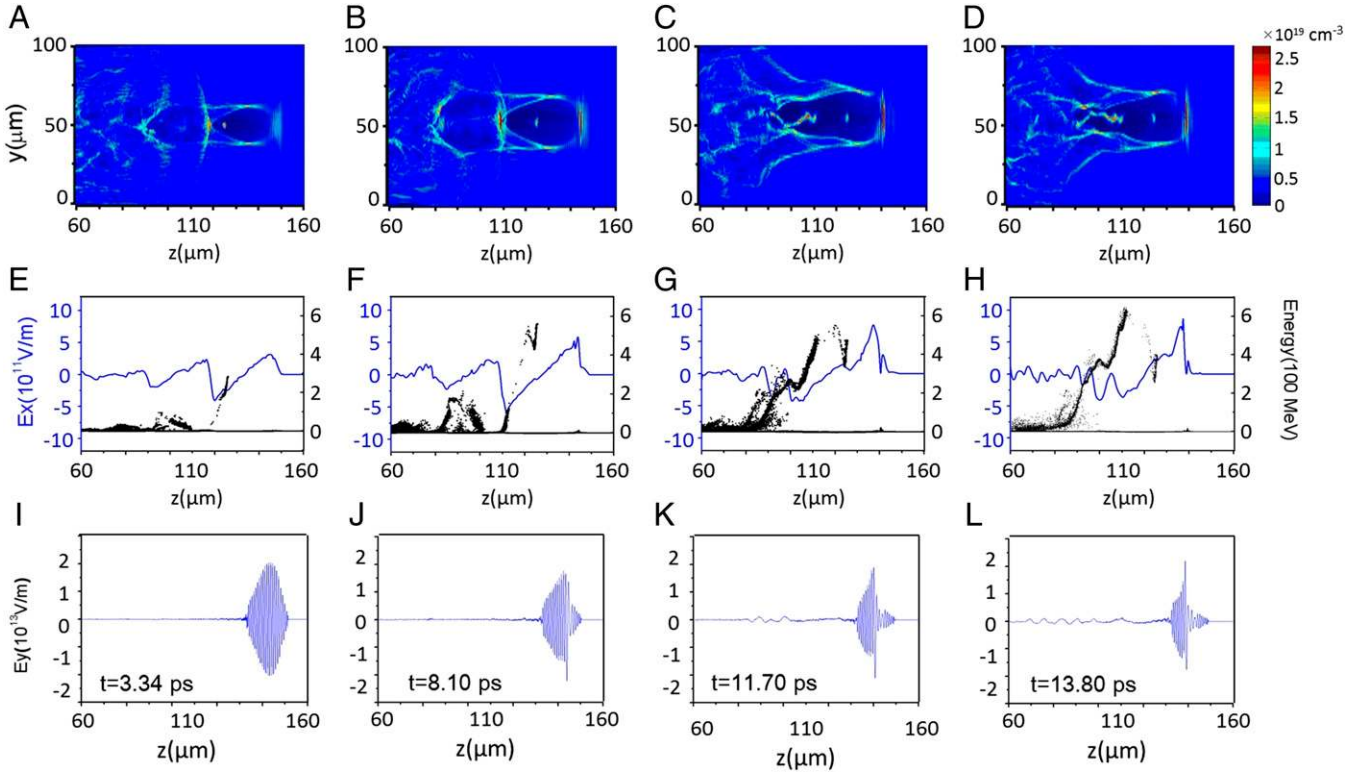

Fig. 3. Typical snapshots of 2D-PIC simulation results. Frames *A*, *E*, and *I* correspond to the time $t = 3.34$ ps; frames *B*, *F*, and *J*, to $t = 8.10$ ps; frames *C*, *G*, and *K*, to $t = 11.70$ ps; and frames *D*, *H*, and *L*, to $t = 13.80$ ps; *A–D* are the electron density distributions, and *E–H* are the kinetic energy of the electrons (black dots) and the longitudinal electric fields (blue lines). The longitudinal profiles of the laser electric fields are shown in *I–L*. The incident laser peak amplitude is $a_0 = 3.6$.

experiment (Fig. 2*E*). During the first bunch dephasing, the second bunch is still in its acceleration phase and finally results in a much higher energy. The energy evolution of two electron bunches is summarized in Fig. 5, both for experiment and simulation (*Inset* of Fig. 5), and good agreement is evident. Therefore, the OBI mechanism can explain well the second electron bunch and corresponding high-flux betatron radiation observed in the experiment.

It is experimentally demonstrated that the second injected electron bunch is correlated to the emergence of intense betatron X-ray emission. Fig. 5 shows the X-ray photon flux measured in the experiment and calculated for small (0.4-μm) and large-amplitude (4-μm) betatron oscillations related to the first and second electron bunches correspondingly. The calculated photon number from different amplitudes can be deduced as mentioned in the introduction: The X-ray photon number is given by $N_{ph} = N_e \times N_x$, where N_e is the electron number contribution to the radiation. Let us take laser-plasma channeling length $L = 10$ mm as an example. For the small amplitude, taking $r_0 = 0.4$ μm from simulation and $\gamma = 700$, $n_e = 4 \times 10^{18}$ cm^{-3} from experiment, the plasma wiggler strength parameter $K = 2\pi(\gamma r_0)/\lambda_b = 2.7$, where betatron wavelength $\lambda_b = (2\gamma)^{1/2}\lambda_p = 636$ μm, the number of betatron oscillations executed by an electron in ion channel $N_\beta = L/\lambda_b = 14$. The charge of the quasi-monoenegertic electron bunch (35 pC) in experiment corresponds to 2×10^8 electrons. So the average number of photons can be calculated to be $N_{ph} = 4.5 \times 10^7$ photons. For the large amplitude, taking $r_0 = 4$ μm from simulation at this position and $\gamma = 2{,}800$, $n_e = 4 \times 10^{18}$ cm^{-3} according to the experiment, we obtain $K = 56.3$, $\lambda_b = 1{,}272$ μm, $N_\beta = 7$. The calculated photon number is $N_{ph} = 4.6 \times 10^8$ with the same experimental electron charge. As shown in Fig. 5, measured and calculated (for 4-μm amplitude) photon flux increase monotonically following the evolution of the second electron bunch. The calculated flux (green dashed line) for 0.4-μm amplitudes is far lower than what we observed experimentally. The results in Fig. 5 clearly show that intense and highly collimated X-ray emission can be ascribed mainly to the second-injected electron bunch due to its high-energy and large transverse

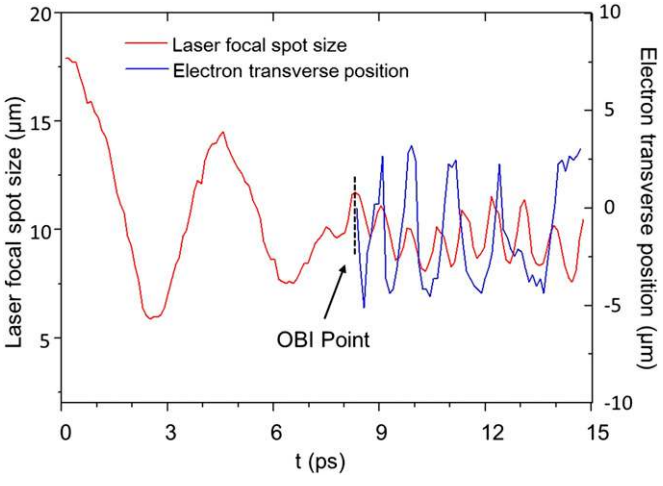

Fig. 4. The time evolution of the laser beam size and the transverse electron oscillations. Initially, the laser spot oscillates slowly until around $t = 8$ ps when the oscillation period drops dramatically. The injection due to the oscillating bubble (for the second electron bunch) starts afterward, which is accompanied by the resonantly enhanced transverse oscillations of the trapped electron bunch (blue curve).

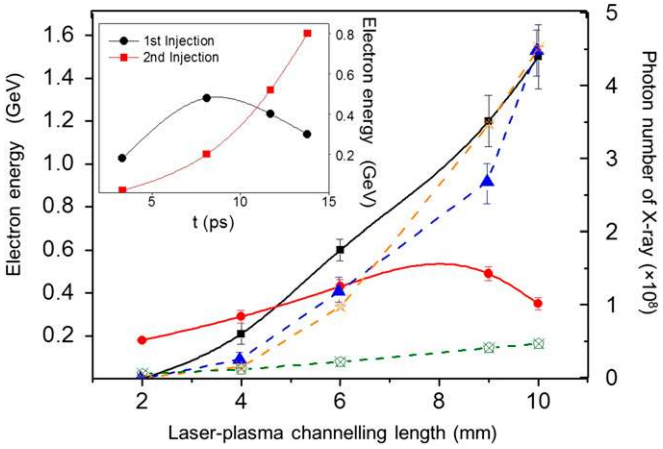

Fig. 5. Scaling of electron energy and betatron X-ray photon number versus the channel length. The red solid curve shows the central energy of the first injected electron bunch, whereas the black solid curve represents the cutoff (max.) energy of the second injected bunch found from the experiment; the blue dashed curve is the X-ray photon number from the experiment; the yellow dashed curve and the green dashed curve give the photon numbers calculated by assuming betatron oscillations with a small amplitude and large amplitude, respectively. For comparison, the *Inset* plots the temporal dependence of the central energy of the first injected electron bunches and the cutoff energy of the second injected electron bunches obtained from simulation.

oscillation amplitude. Moreover, based on the simulation, one may estimate the pulse duration of the betatron radiation to be around 30 fs, which is the beam length of the high-energy part of the second electron bunch, as shown in Fig. 3. The simulation reveals that the source size estimated from the amplitudes of the electron oscillation is ~6 μm. Hence, the peak brightness of the betatron source is 1.2×10^{23} photons·s^{-1}·mm^{-2}·mrad^{-2}·(0.1%) bandwidth^{-1}.

In conclusion, we have reported experimental observation of simultaneous generation of two energetic electron bunches and bright betatron X-ray emission. The two electron bunches have distinct features, one with a quasi-monoenergetic peak at about 300 MeV and another with a continuous spectrum extending up to over 1 GeV and with a large divergence angle. The betatron X-ray emission is associated with the second electron bunch emerging at later time when significant evolution of the laser pulse appears. The violent oscillations of the laser spot size lead to OBI, which produces the second electron bunch with large betatron oscillation amplitudes for bright betatron X-ray radiation. Our results suggest a way toward the concurrence of high-quality monoenergetic electron beams and bright betatron X-rays in a single-shot laser wakefield accelerator. This is potentially interesting for "single-shot" ultrafast X-ray/electron pump–probe applications, such as phase contrast imaging, X-ray absorption fine structure, and X-ray diffraction studies of warm dense matter with femtosecond time resolution.

Materials and Methods

Laser System. The experiments were performed at the Jupiter Laser Facility, Lawrence Livermore National Laboratory, using the Callisto laser system. This Ti:sapphire system can delivers up to 200 TW in power in a 60-fs laser pulse at the central wavelength λ_0 of 806 nm. The laser pulse was focused with an *f*/12 off-axis parabolic mirror to a vacuum spot of 18 μm in diameter with 35% energy contained at the full width at half-maximum (FWHM). During the experiments, the peak laser power ranged from 60 to 155 TW on the target. In the focused region, the laser intensity was $I = 1.1 \times 10^{19}$ to 3.0×10^{19} W·cm^{-2}, which corresponded to the normalized vector potential $a_0 = 2.3{\sim}3.8$, where $a_0 = 8.6 \times 10^{-10}\ \lambda[\mu m]I^{1/2}[W/cm^2]$.

Gas Jet. A supersonic helium gas jet nozzle was used, which is commercially available (31). It has a rectangular shape of 10 mm in length and 1.2 mm in width, capable of produces a supersonic gas flow with a Mach number ~5. The gas densities generated from the gas jet were characterized using fluid dynamic calculations from the manufacturer (31). The gas jet can generate well-defined uniform gas density profiles in the range of $1 \times 10^{18} \sim 3 \times 10^{19}$ cm^{-3} by changing the helium stagnation pressure. The laser was focused in vacuum at the front edge of the nozzle and at the height of 2 mm above the nozzle.

Diagnostics of Electron Beams and X-Ray Radiation. A 16-cm-long 0.98-T dipole magnet, which was centered 112 cm from the exit of the gas jet, was set to disperse the electron beams. Four image plates (Fuji BAS-SR) were arranged as shown in Fig. 1. Image plate 1 was placed to get the profile information of the electrons without the magnet. Image plate 2 was pasted on the side of the magnet to measure the electron energy spectrum from 6 to 100 MeV. Image plates 3 and 4 were located at 155 and 205 cm away from the exit of the gas jet, respectively, which provided unambiguous energy spectrum measurement of the high-energy electrons (8, 32). A 1.5-mm-thick Be-window was used to seal the vacuum. This setup provided a total error in energy of 2.5% at 500 MeV. The published calibration of the image plate's photo-stimulated luminescence provided information on the electron beam charge and the betatron photon flux (33, 34). Various filters (1.5-mm-thick Be-window, 30-μm Al foils, 350-μm-thick image plate, and 55-cm air) between the gas jet and image plate 3 allowed the detection of X-ray photons of >7 keV in energy. To obtain the critical energy of the X-rays, we use the calculated transmission of X-rays through the different metal filters with a least squares (23). To monitor the interaction volume, a charge-coupled device (CCD) with a low-pass filter was used to observe harmonic emission of the target. This device measured the Thomson scattering to determine the interaction position and the time-integrated plasma channel length.

Particle-in-Cell Simulation. The 2D-PIC simulations were performed using parameters that matched the experimental values with the code OOPIC, where a p-polarized laser pulse with duration of $\tau_{FWHM} = 60$ fs was focused into a pure gas target with a focal spot size of $w_0 = 18$ μm. A laser pulse with a normalized peak electric field of $a_0 = 2.3{\sim}3.8$ was launched at the entrance of the plasma of uniform helium density at 4×10^{18} cm^{-3}. The laser pulse was assumed to have a perfect transverse Gaussian-shaped envelope.

ACKNOWLEDGMENTS. We thank R. Cauble, S. Maricle, J. Bonlie, and other Jupiter Laser Facility staffs at Lawrence Livermore National Laboratory (LLNL) for laser and technical support and Joseph Nilsen for facilitating the experiment. This work was supported by the National Basic Research Program of China Grants 2013CBA01501 and 2013CBA01504, National Key Scientific Instrument and Equipment Development Project 2012YQ120047, and National Natural Science Foundation of China Grants 11334013, 11121504, 11220101002, 11175119, and 11374209. Part of this work was performed under the auspices of the US Department of Energy by LLNL under Contract DE-AC52-07NA27344.

1. Vainshtein BK (1991) Diffraction investigation of the atomic-structure of matter. *Acta Crystallogr B* 47:145–154.
2. Tajima T, Dawson JM (1979) Laser electron-accelerator. *Phys Rev Lett* 43(4):267–270.
3. Faure J, et al. (2004) A laser-plasma accelerator producing monoenergetic electron beams. *Nature* 431(7008):541–544.
4. Geddes CGR, et al. (2004) High-quality electron beams from a laser wakefield accelerator using plasma-channel guiding. *Nature* 431(7008):538–541.
5. Mangles SPD, et al. (2004) Monoenergetic beams of relativistic electrons from intense laser-plasma interactions. *Nature* 431(7008):535–538.
6. Leemans WP, et al. (2006) GeV electron beams from a centimetre-scale accelerator. *Nat Phys* 2(10):696–699.
7. Hafz NAM, et al. (2008) Stable generation of GeV-class electron beams from self-guided laser-plasma channels. *Nat Photonics* 2(9):571–577.
8. Clayton CE, et al. (2010) Self-guided laser wakefield acceleration beyond 1 GeV using ionization-induced injection. *Phys Rev Lett* 105(10):105003.
9. Corde S, et al. (2013) Observation of longitudinal and transverse self-injections in laser-plasma accelerators. *Nat Commun* 4:1501.
10. Kim HT, et al. (2013) Enhancement of electron energy to the multi-GeV regime by a dual-stage laser-wakefield accelerator pumped by petawatt laser pulses. *Phys Rev Lett* 111(16):165002.
11. Wang XM, et al. (2013) Quasi-monoenergetic laser-plasma acceleration of electrons to 2 GeV. *Nat Commun* 4:1988.
12. Esarey E, Shadwick BA, Catravas P, Leemans WP (2002) Synchrotron radiation from electron beams in plasma-focusing channels. *Phys Rev E Stat Nonlin Soft Matter Phys* 65(5 Pt 2):056505.
13. Németh K, et al. (2008) Laser-driven coherent betatron oscillation in a laser-wakefield cavity. *Phys Rev Lett* 100(9):095002.

14. Nakajima K, et al. (2011) Operating plasma density issues on large-scale laser-plasma accelerators toward high-energy frontier. *Phys Rev Spec Top-Ac* 14(9):091301.
15. Schoenlein RW, et al. (1996) Femtosecond X-ray pulses at 0.4 angstrom generated by 90 degrees Thomson scattering: A tool for probing the structural dynamics of materials. *Science* 274(5285):236–238.
16. Spielmann C, et al. (1997) Generation of coherent X-rays in the water window using 5-femtosecond laser pulses. *Science* 278(5338):661–664.
17. Chen LM, et al. (2008) Study of x-ray emission enhancement via a high-contrast femtosecond laser interacting with a solid foil. *Phys Rev Lett* 100(4):045004.
18. Chen LM, et al. (2010) Intense high-contrast femtosecond K-shell x-ray source from laser-driven Ar clusters. *Phys Rev Lett* 104(21):215004.
19. Schlenvoigt HP, et al. (2008) A compact synchrotron radiation source driven by a laser-plasma wakefield accelerator. *Nat Phys* 4(2):130–133.
20. Fuchs M, et al. (2009) Laser-driven soft-X-ray undulator source. *Nat Phys* 5(11): 826–829.
21. Kneip S, et al. (2010) Bright spatially coherent synchrotron X-rays from a table-top source. *Nat Phys* 6(12):980–983.
22. Cipiccia S, et al. (2011) Gamma-rays from harmonically resonant betatron oscillations in a plasma wake. *Nat Phys* 7(11):867–871.
23. Rousse A, et al. (2004) Production of a keV x-ray beam from synchrotron radiation in relativistic laser-plasma interaction. *Phys Rev Lett* 93(13):135005.
24. Mangles SPD, et al. (2009) Controlling the spectrum of x-rays generated in a laser-plasma accelerator by tailoring the laser wavefront. *Appl Phys Lett* 95(18):181106.
25. Chen LM, et al. (2013) Bright betatron X-ray radiation from a laser-driven-clustering gas target. *Sci Rep* 3:1912.
26. Lu W, et al. (2007) Generating multi-GeV electron bunches using single stage laser wakefield acceleration in a 3D nonlinear regime. *Phys Rev Spec Top-Ac* 10(6): 061301.
27. Kneip S, et al. (2009) Near-GeV acceleration of electrons by a nonlinear plasma wave driven by a self-guided laser pulse. *Phys Rev Lett* 103(3):035002.
28. Tajima T (1985) High-energy laser plasma accelerators. *Laser Part Beams* 3:351–413.
29. Pukhov A, Meyer-ter-Vehn J (2002) Laser wake field acceleration: The highly non-linear broken-wave regime. *Appl Phys B* 74(4-5):355–361.
30. Faure J, et al. (2005) Observation of laser-pulse shortening in nonlinear plasma waves. *Phys Rev Lett* 95(20):205003.
31. Hosokai T, et al. (2002) Supersonic gas jet target for generation of relativistic electrons with 12 TW-50 fs laser pulse. *Proceedings of the Eighth European Particle Accelerator Conference* (European Physical Society Interdivisional Group on Accelerators and CERN, Geneva), pp 981–983.
32. Pollock BB, et al. (2011) Demonstration of a narrow energy spread, ~0.5 GeV electron beam from a two-stage laser wakefield accelerator. *Phys Rev Lett* 107(4):045001.
33. Nakanii N, et al. (2008) Absolute calibration of imaging plate for GeV electrons. *Rev Sci Instrum* 79(6):066102.
34. Mao JY, et al. (2012) Application of a transmission crystal x-ray spectrometer to moderate-intensity laser driven sources. *Rev Sci Instrum* 83(4):043104.